Council on Tall Buildings and Urban Habitat Korea

International Journal of
High-Rise Buildings
www.ctbuh-korea.org/ijhrb/index.php

International Journal of High-Rise Buildings
September 2022, Vol 11, No 3, 145-156
https://doi.org/10.21022/IJHRB.2022.11.3.145

Application Examples of CFD at the Planning Stage of High-Rise Buildings

Hiroto Kataoka[1†], Yoshiyuki Ono[1], Kota Enoki[1], Yuichi Tabata[1], and Satoko Kinashi[1]

[1]*Technology Research Institute, Obayashi Corporation, Japan*

Abstract Application examples of computational fluid dynamics (CFD) in the planning stage of high-rise buildings are introduced. First, we introduce examples of applications in the environmental field. The pedestrian wind environment was one of the earliest practical examples of CFD. CFD was also employed to validate the heat island mitigation measures proposed as part of the new construction plan. Second, application examples of wind-force evaluations are introduced. Prediction examples are presented for the peak wind pressure around a complex-shaped building and the wind force evaluation for a base-isolated building. The results prove that the results of the proper execution of CFD are equivalent to those of the wind tunnel experiment. As examples of CFD applications of other issues related to high-rise building planning, we introduce snow accretion on outer walls and high-temperature exhaust from emergency generators. Finally, the future prospects for the use of CFD are discussed.

Keywords CFD application, environmental simulation, heat island mitigation measures, wind force evaluation, snow accretion on claddings.

†Corresponding author:
Hiroto Kataoka
Tel: +81-42-495-4934
E-mail:
kataoka.hiroto@obayashi.co.jp

1. Introduction

Computational fluid dynamics (CFD) is a method of discretizing a basic equation describing a flow field and numerically solving it using a computer. Provided that sufficient computing power and appropriate software are utilized, CFD can reproduce the airflow and scalar (for example, temperature) distribution without requiring large-scale experimental devices, such as wind tunnels.

With respect to computing power, the computing speed of PCs has greatly improved, to say nothing of high-performance computers (HPCs). The most powerful HPC continues to be about 10 times faster in five years. Commercially available CFD codes are widespread. They have been advancing their numerical methods and ease of use. Moreover, open-source code CFD software, such as OpenFOAM, has attracted attention. Above all, it is very appealing that no fees are levied for use.

Owing to the unprecedented progress in hardware and software and the development of computational methods, it can be stated that CFD has reached the level where it is practically used from a technical perspective.

Numerous preliminary studies have been conducted during the early stages of high-rise building planning. Some of these require further experimentation. In experiments, it is difficult to examine many cases owing to the cost constraints. Ideally, it is desirable to perform preliminary studies of many cases using numerical simulation, and based on the results, conduct experiments for the minimum number of cases required.

In this paper, application examples of CFD at the planning stage of high-rise buildings are introduced. Some examples are cited from the author's previous paper (Kataoka, Ono and Enoki, 2020) which consists of applications for environment flows and wind force evaluations. Some results are compared with experimental results and examined for their applicability to practical tasks, especially for the planning stage of high-rise buildings. Finally, future prospects are discussed.

2. Environmental Simulations

2.1. Assessment for pedestrian wind environment

CFD has become one of the most practical tools for assessing pedestrian wind environments around high-rise buildings. To overcome such tedious tasks as modeling the shape of project buildings and their surroundings from maps or design drawings and generating a computational grid system around them, they should be simplified while

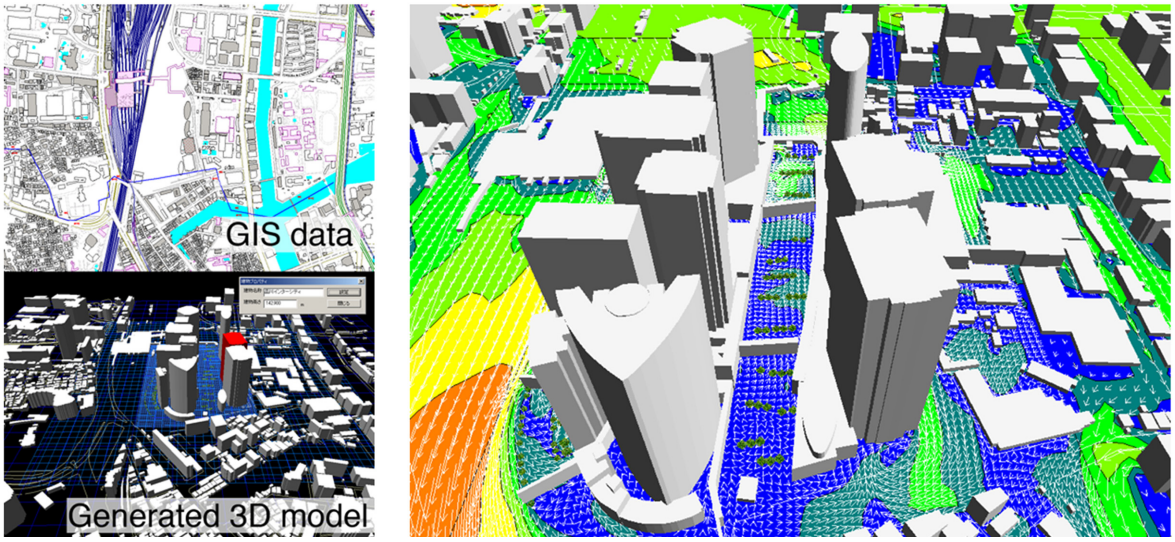


Figure 1. 3D modeling from GIS data (left) and computed wind flows near ground surfaces (right).

maintaining the accuracy of the solution. The advent of digital maps and geographic information systems (GIS) has made the modeling process easier and more efficient. The adoption of an overlapping equidistant Cartesian grid system makes it easier to control the local grid density, and allows for simpler code programming than other discretizations. Figure 1 explains how we generated threedimensional (3D) building models from GIS data and illustrated the computed wind flows around buildings (Kataoka, Kinashi and Kawaguchi, 2002). Wall surfaces that did not coincide with grid lines were treated by the FVOR method by Hirt (1992), and the effects of windbreak trees were simulated using the tree canopy model presented by Kato *et al.* (2001). The effect of turbulence was modeled by the standard k-e model of the Reynolds-averaged Navier-Stokes simulation (RANS). Table 1 presents the outline of the wind environment simulator "Zephyrus®".

The solution accuracy was confirmed with the results submitted to a cooperative project for CFD prediction of a pedestrian wind environment at the Architectural Institute of Japan (AIJ). Some of the results are presented in Yoshie *et al.* (2007). Prediction accuracy was guaranteed by the AIJ guidelines (Tominaga *et al*., 2008).

The simulated velocity values were normalized by the speeds of the reference point (e.g., the nearest weather station), and their statistical properties were reproduced via the Weibull parameters obtained from the observation data at the reference point. The criteria proposed by Murakami *et al*. (1983) to assess the wind environment are most frequently used. They are based on the excess probabilities of the day maximum instantaneous wind speed. The day maximum of instantaneous wind speeds can be approximated by multiplying the day maximum of the 10-minute averaged speeds by the gust factor. Equation 1 indicates how the excess probability of the day maximum instantaneous wind speed P ($> V$) is estimated from the normalized speed R (a) computed for each wind direction a by using Weibull parameters C (a) and K (a). V denotes the daily maximum instantaneous wind speed, A (a) indicates the occurrence probability of the wind direction, and G (a) represents a gust factor.

$$P(>V) = \sum_{a=\mathrm{NNE}}^{\mathrm{N}} A(a) exp\left\{-\left(\frac{V}{C(a)R(a)G(a)}\right)^{K(a)}\right\} \quad (1)$$

Table 1. Outline for the wind environment simulator "Zephyrus®"

Item	Description
Solution algorithm	Artificial compressibility method + Dual time stepping.
Discretization	Finite Volume Method (FVM), Collocated grid storage. Orthogonal + Overlapping grid system. Equidistant in horizontal direction and stretched in vertical.
Time integration scheme	RANS: steady computation, LES: 2nd-order implicit.
Spatial differentiation	3rd-order upwind scheme for convective term. 2nd-order central difference scheme for other terms.
Turbulence model	RANS: standard *k*-ε, Kato-Launder, Duribin, S-Ω. LES: no SGS model (Implicit LES).
Wall boundary condition	RANS: wall function, LES: no-slip.
Tree canopy model	RANS: Kato *et.al*. (2001), LES: unavailable.

Depending on the neighboring conditions, the value of the gust factor is set in the range of 1.5 to 3. Although the gust factor has a significant influence on the evaluation results, there was no reasonable method to determine its value. Therefore, based on the wind speed measurements of 15 sites in Tokyo, we proposed an evaluation equation for the gust factor, as shown in Equation 2 (Kinashi *et al.*, 2005).

$$G(a) = 1.41\left(\frac{Z_R}{Z_G}\right)^{-0.44\alpha} R(a)^{-0.44}, \quad G(a) \leq 4.2 \quad (2)$$

Z_R denotes the evaluation height, and Z_G indicates the boundary layer height defined in the AIJ Recommendations for Loads on Buildings (hereinafter referred to as RLBAIJ) (2015) according to the terrain roughness category.

Approximately 10~20 projects per year are simulated using CFD. CFD is mainly used for small projects that cannot meet the experimental expenses. It is also implemented for large-scale projects, particularly in the early design stages before conducting wind tunnel experiments. CFD is not a replacement for wind tunnel experiments; instead, they are mutually complementary.

2.2 Usability of the rooftop garden of a high-rise building

In recent years, the number of outdoor facilities installed around high-rise buildings has increased. The availability of outdoor facilities is susceptible to weather conditions. In particular, for stores and event plazas, annual total business hours are directly linked to profits. Therefore, it is expected that specific information will be provided based on reliable weather forecasts from the planning stage. Accordingly, the wind speed values at which these facilities can be operated and the tolerances for guests or users were pre-determined based on outdoor facilities and activities (Kinashi *et al.*, 2018). Subsequently, the available time per year was predicted based on the daily wind speed computed by CFD at the location of each facility.

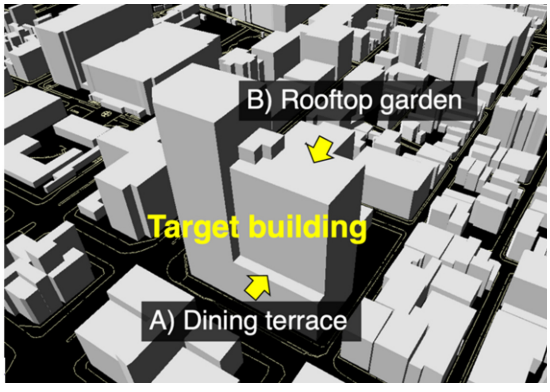


Figure 2. CFD model of the target building.

Figure 2 illustrates an example of usability evaluation. Outdoor facilities are planned on the middle floor (A: dining terrace with a height of 35 m) and top floor (B: rooftop garden with a height of 100 m) of a high-rise building (height 130 m) in Tokyo (Kinashi *et al.*, 2018). For the reference wind, 10-minute-average values for every 10-minutes for five years (2012-2016) of the Tokyo Meteorological Observatory were used. The total number of data points is 263,088. The time-averaged wind velocities were computed using CFD for each wind direction at a pitch of 22.5° under constant wind speed conditions. The computed values were then converted into time-series values based on the observation record of the wind direction and speed at the observatory. Lastly, the instantaneous wind speeds during business hours (9:00-21:00) were obtained by multiplying by the gust factor.

Figure 3 shows the time and cumulative frequency of instantaneous wind speeds at the representative points of each facility. The dining terrace is in winter and the rooftop garden is in summer. When the instantaneous wind speed is less than 5 m/s, more than 50% of guests eat and drink outdoors. Therefore, if the thermal conditions are satisfied, the dining terrace will operate for approximately 61% of the season. When the instantaneous wind speed exceeds 6 m/s, the banners and poles used in outdoor activities sway violently. Therefore, we found that 52% of the summer business hours in the rooftop garden are suitable for use

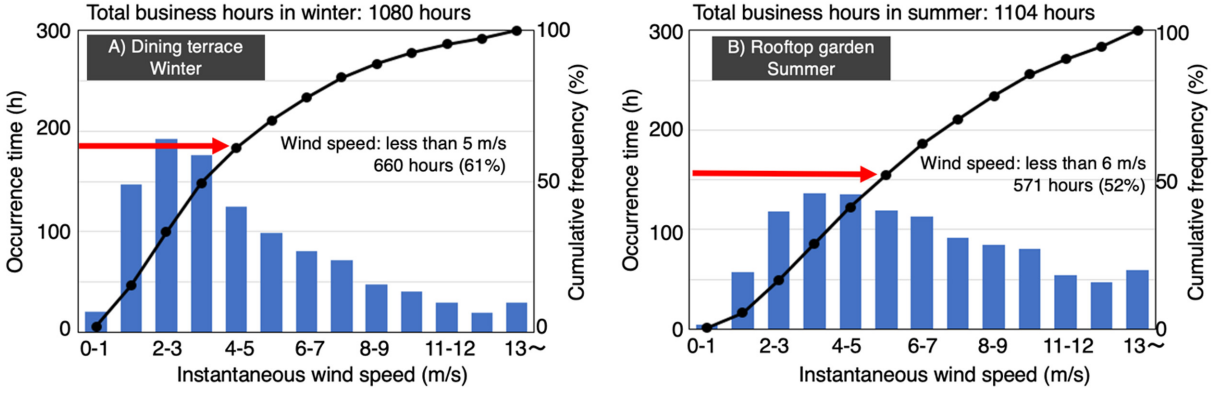


Figure 3. Occurrence time and cumulative frequency of instantaneous wind speeds by wind speed class at the representative points of each facility (2 m above the floor).

with these tools. Moreover, we also found that installing a 5 m high glass wall around the roof garden could extend the available time of these tools.

2.3 Outdoor thermal environments

The rising temperatures in urban areas due to the heat island phenomenon pose problems for people residing or working in these areas, and various measures have been proposed to mitigate its adverse effects. When mitigation measures are proposed as part of new building plans, their validity can be enhanced if the public can understand how such measures bring about quantitative improvement in the outdoor environment. To fulfil this demand, we have developed a numerical urban climate simulator, as described below.

Figure 4 presents the computed results of the outdoor thermal environment in the summer for an existing urban area covered by high-rise buildings (Kataoka *et al.*, 2009). The entire domain size was 1.3 km × 1.4 km × 0.7 km high. The horizontal grid resolution was set to 10 m and

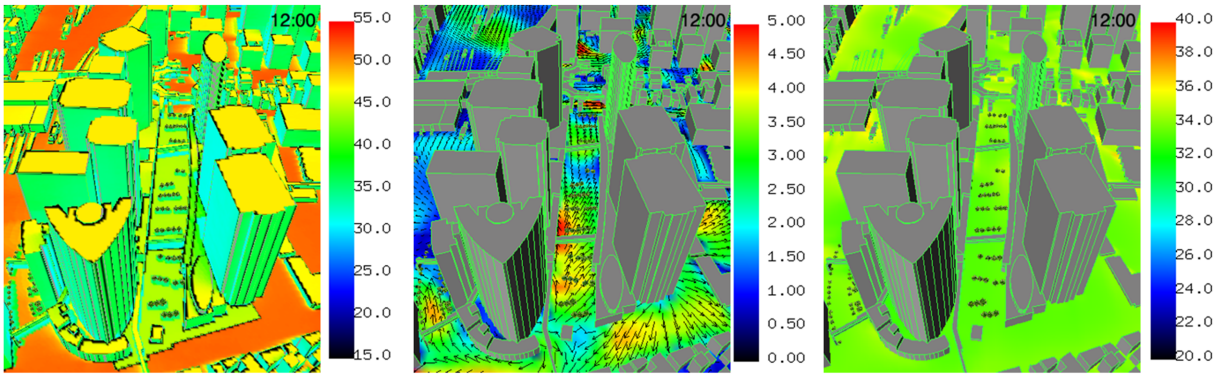
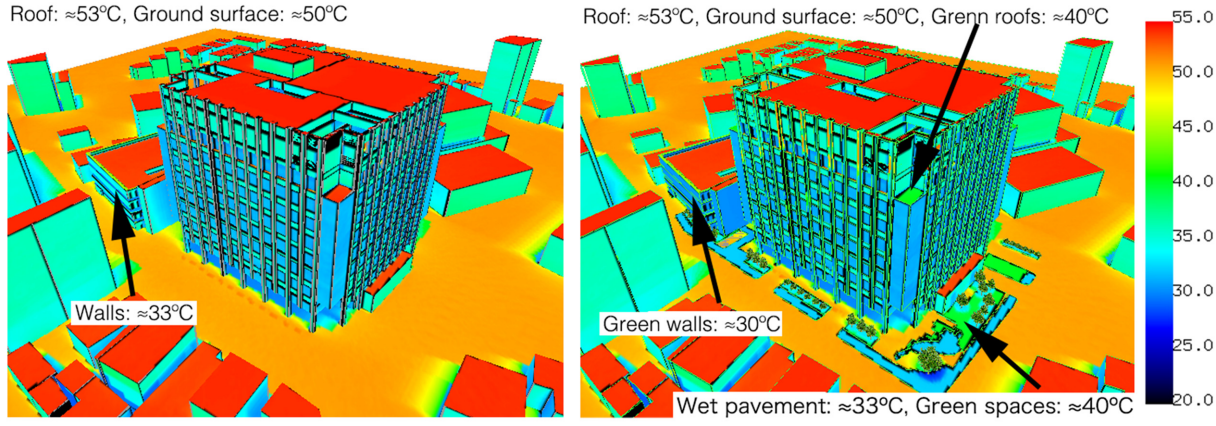
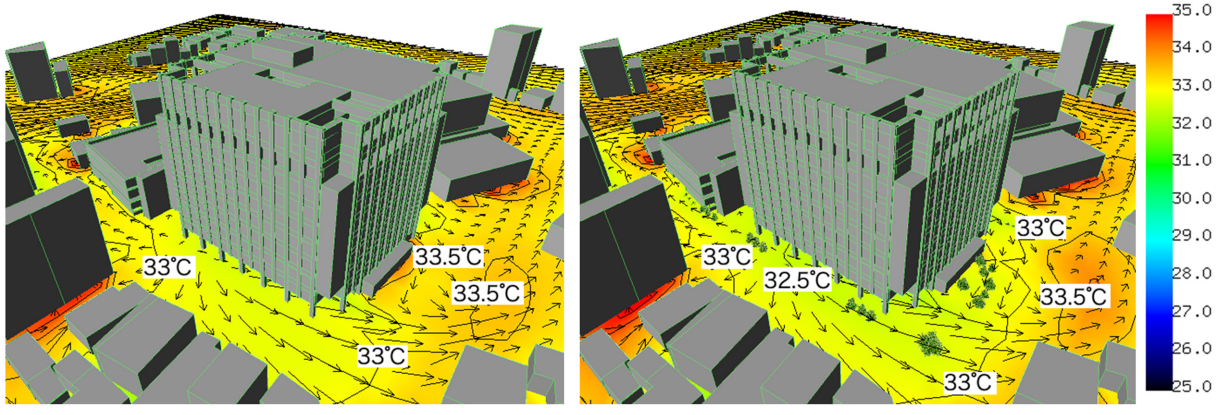


Figure 4. Forecast example of outdoor thermal environment in summer.



a) Wall surface temperature [°C] with no mitigation measures (left) or mitigation measures (right).



b) Air temperature (GL+1.5m) [°C] with no mitigation measures (left) and mitigation measures (right).

Figure 5. Predicted effects of heat island mitigation measures.

the vertical resolution was 2~100 m. The wall surface temperature was obtained by calculating the solar radiation and infrared radiation between the buildings under uniform air temperature and wind velocity conditions. Subsequently, the distributions of the wind velocity, air temperature, and absolute humidity were computed using the surface temperature as a boundary condition. An improved Mellor–Yamada closure model proposed by Nakanishi (2001) was employed to compute turbulence fluxes. Temperature and absolute humidity were computed on the surface of the tree leaves, assuming convective heat transfer and latent heat release, convective water vapor transfer, and transpiration from the pores were balanced.

As shown in Figure 4, ground surface temperatures differed significantly between the paved and revegetated areas. Air temperatures appeared to be lower near trees and higher in blowdown areas with lower wind speeds.

Using this calculation method, the effectiveness of heat island mitigation measures, such as mist spraying, humidification of road surfaces, and greening of building wall surfaces, have been confirmed for a middle-sized building plan, as depicted in Figure 5. Evidently, the surface temperature of a portion of the rooftop and wall surface was lowered by greening. Greening and wet paving around the building can also lower the air temperature by approximately 0.5°C to 1°C. Thus, it is possible to evaluate the positive impact of the project on the surrounding city blocks by evaluating the effects of heat island measures in advance. However, it is difficult to perform accurate quantitative verification because the thermal boundary conditions cannot be set exactly the same in real phenomena and analytical models.

2.4 Flow within urban canopy

The heat island phenomenon is mitigated if the wind flow within an urban canopy is sufficient to blow heat downwind. This concept is called an urban ventilation path. The existing urban area is composed of buildings of various heights that irregularly cover the surface of the Earth. The shape of such a complex city governs the vertical distribution of wind speed, which has a significant effect on the wind load acting on high-rise buildings.

RLBAIJ (AIJ, 2005) regulates the velocity profile based on the terrain roughness category. As the definition of the roughness category is ambiguous, it may be difficult to determine the category to which the target area belongs. Therefore, Large Eddy Simulation (LES) calculations were performed to investigate the relationship between the power law index of the vertical wind velocity profile and the roughness parameter of a real urban area where the height and arrangement of buildings are randomly distributed (Kataoka and Tamura, 2014).

The instantaneous scalar velocity distributions are displayed in Figure 6. A rectangular area 2 km wide × 19.5 km long × 2 km high from Tokyo Bay to the inland area was developed. It was discretized using an equidistant orthogonal grid system in the horizontal plane with a resolution of 10 m × 10 m, and a non-equidistant grid system in the vertical direction with a resolution of 2 to 300 m (200 × 1,950 × 63 = approximately 24.5 million volume elements). Near the ground surface, the velocity decreased rapidly across the coastline but recovered over parks and rivers. At an altitude of 105 m, the velocity decreases approximately 2 km leeward from the coastline and does not exhibit such local recovery as velocity distributions near the ground surface.

The computed results were confirmed by the observation data obtained by a Doppler light detection and ranging (LiDAR) system under neutral atmospheric conditions, as shown in Figure 7. The velocity profiles were normalized by a magnitude of Z_G = 500 m. These three (computed and observed) velocity profiles coincided at a height of Z = 200-500 m, which confirmed the validity of the present LES.

Figure 8 shows changes of the power law index a by LES and the estimated values presented from roughness parameters along with the wind-directional centerline of the target domain. The index a is averaged over 200~400 m. The estimation is based on the tallest building height, the variation of the building height, and a limit height where the roughness density evaluated from the top exceeds 0.1. The figure illustrates the results of two different estimations; however, the differences between them are small and coincide well with LES. For more

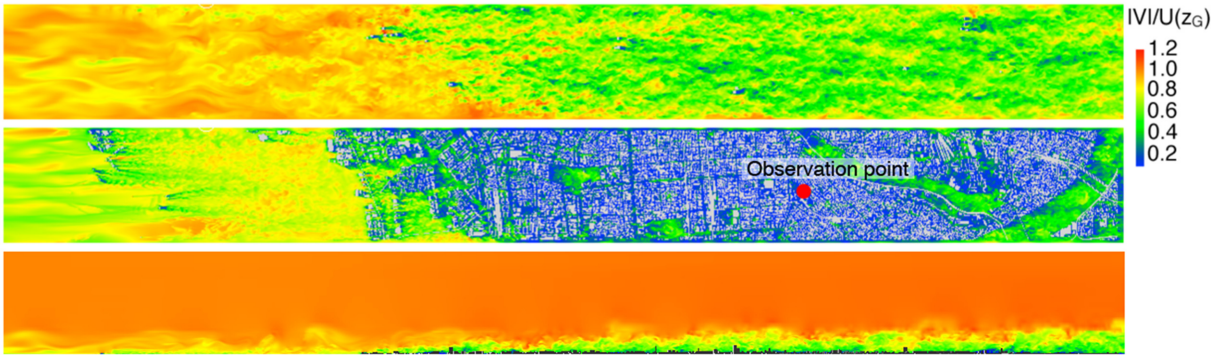


Figure 6. Instantaneous distributions of scalar wind velocity. (z = 105 m, 5 m and vertical section)

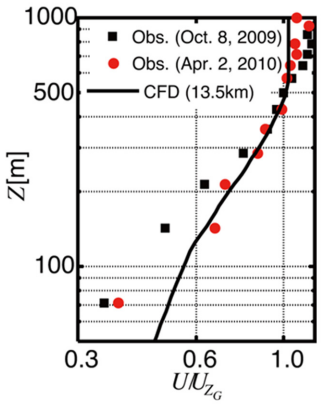


Figure 7. Validation of LES by observation data.

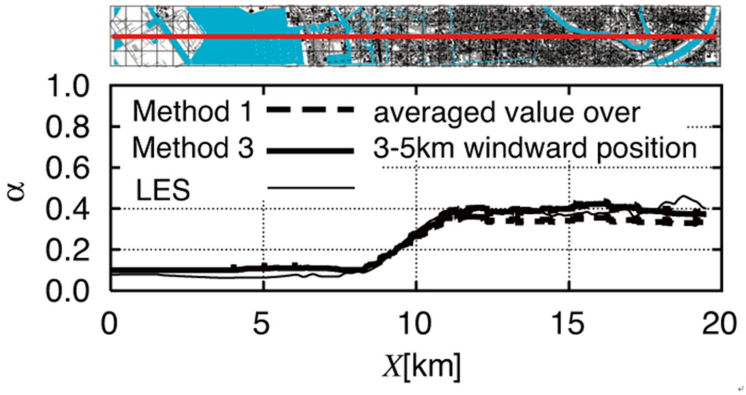


Figure 8. Estimated power law index by roughness parameters.

detail of the estimation method, please refer to our previous study (Kataoka and Tamura, 2014).

3. Wind force evaluation

3.1 Peak wind pressure distributions of a building having complicated surfaces

An evaluation of the wind load acting on a building with complex-shaped surfaces by LES using an unstructured grid system was introduced. The applicability of the LES wind load assessment was verified by comparing the results with the wind tunnel experiments.

Table 2 outlines the LES solver using unstructured grids (Kataoka, Ono and Enoki, 2020). The change in the wind direction was realized by fixing the outer grid block with the inflow boundary and rotating the inner cylindrical block, including the target building. The physical quantity at the interface was interpolated to avoid sharing identical grid points at the interface between the blocks.

Figure 9 presents experimental and LES models to be investigated as a high-rise residential building (Enoki and Ono, 2016). In the experimental model, details such as eaves and irregular outer-wall shapes of lower floors, exposed columns and beams, and balcony floors were

Table 2. Outline for LES code "Aerodyna®" using unstructured grids

Item	Description
Solution algorithm	Fractional step method.
Control volume	Node-centered unstructured finite control volume. 56.4 million grid elements.
Discretization scheme	Crank-Nicolson for time and central difference scheme with 5% artificial viscosity for space.
Orthogonalization correction	Deferred correction.
SGS model	Coherent Structure Smagorinsky model.
Wall boundary condition	Two-layer model (Werner and Wengle).
Wind direction	5 wind directions (270º~350º) at 20º pitch.
CPU	8 cores/node × 384 nodes on K-computer. 14 hours for 7-minute evaluation for each wind direction.

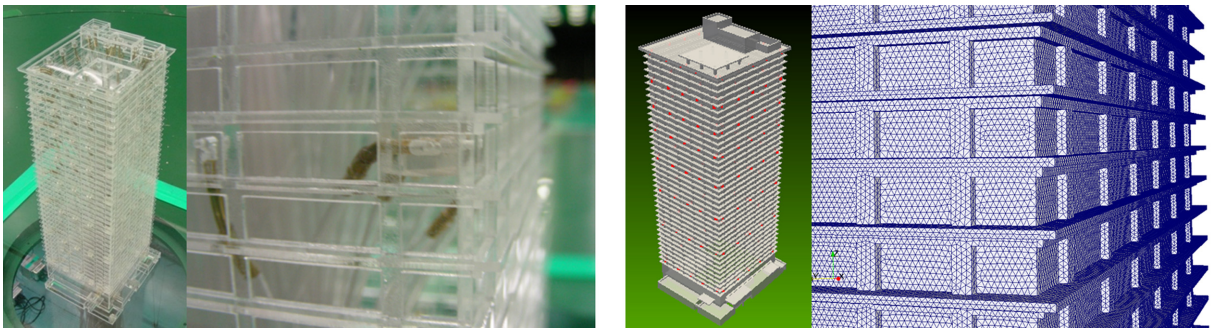


Figure 9. Experimental (left) and computational (right) models for a high-rise residential building. (Aspect ratio: 3.3. Side length ratio: 1.1. Building width: D = 41.35 m.)

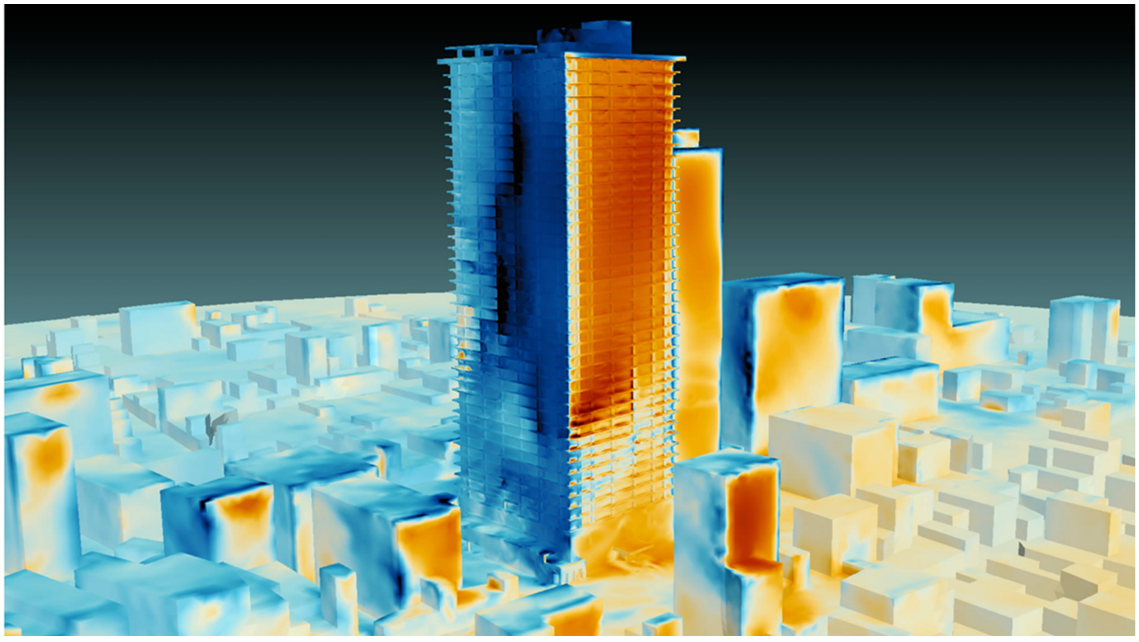


Figure 10. Snapshot of the instantaneous pressure distribution.

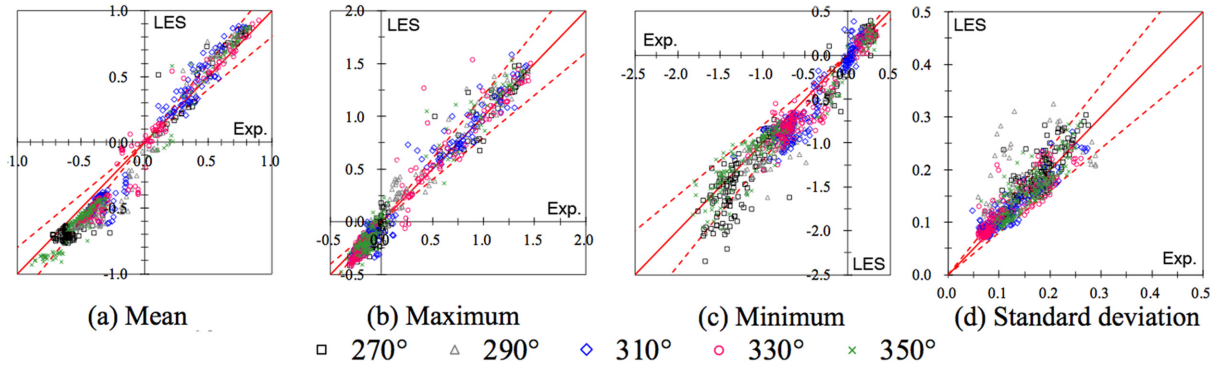


Figure 11. Cross comparisons of pressure coefficients.

reproduced, and these details were also reproduced in the LES model. The computation was performed with five wind directions from 270° to 350° at 20° pitch. The evaluation time was approximately 7 minutes in actual time scale for each wind direction.

Figure 10 shows a snapshot of the instantaneous pressure distribution acting on an entire building. It can be observed that the complex pressure distribution is formed by the balconies and exposed columns. The video clearly shows how the pressure distribution is formed. Figure 11 presents a comparison between the computed and experimental results for the wind pressure coefficients. The mean pressure coefficients deviate from the experimental values at wind direction of 310° and 330°, and the minimum peak deviates at a wind direction of 270°.

Figure 12 shows the surface distribution of the mean pressure coefficient in the 330° wind direction. The hemispheres on the wall indicate the experimental locations of the pressure taps, while their colors signify the difference between the CFD and experimental results. A large difference occurs primarily at the leeward end of the windward surface. Here, separation occurred because of the exposed columns. The slight difference in the shape of the exposed column between the experimental and CFD models may have caused these differences.

Figure 13 illustrates the surface distribution of the minimum peak coefficient in the 270° wind direction. On the side surfaces, strong negative pressure (blue to white) regions were created by flow separation, but appeared sparsely. This is because an insufficient number of ensemble-averaging times (five times for experiments and one for CFD) have been considered because of the computational time. In Figure 13, the low-pressure portion was formed on the windward side of the exposed column. This low-pressure is caused by the formation of a secondary flow upwind along the wall inside the primary separating flow

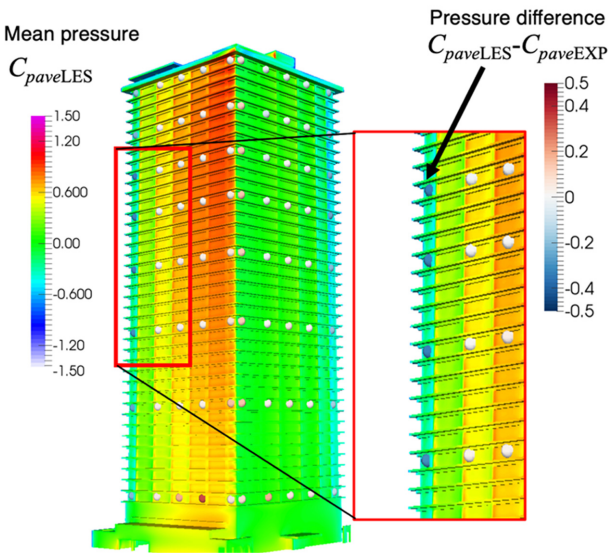


Figure 12. Mean pressure coefficients. (wind direction of 330º)

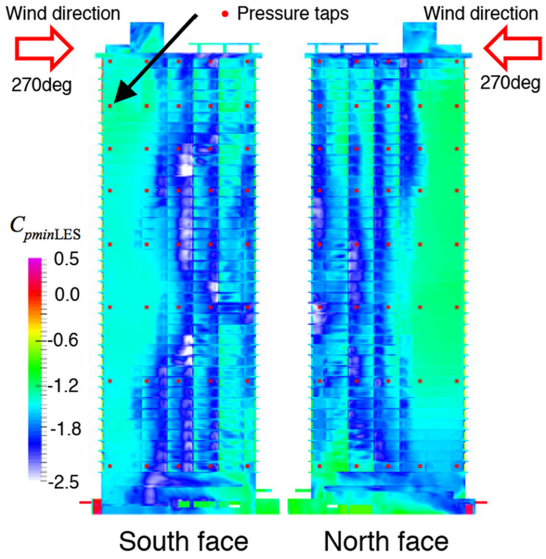


Figure 13. Minimum peak pressure coefficients. (wind direction of 270º)

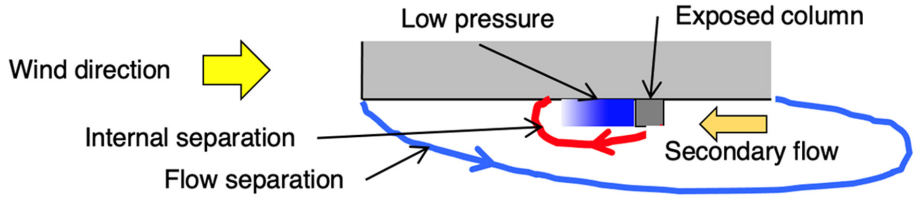


Figure 14. Internal flow separation behind the exposed column.

that covers the entire sidewall, as shown in Figure 14. This secondary flow from the downwind side impinged on the exposed columns, forming an internal separation and low-pressure area on the upwind side.

Figure 15 presents a comparison of the mean wind-force coefficients for all wind directions, including the standard deviation and maximum values, although they are not shown here, the wind tunnel experiment and LES results correspond well.

Evaluations of wind loads acting on buildings with complex-shaped surfaces were performed using LES, and the reproducibility of wind pressure coefficients was verified. The results prove that the results of the proper execution of CFD are equivalent to those of the wind tunnel experiment.

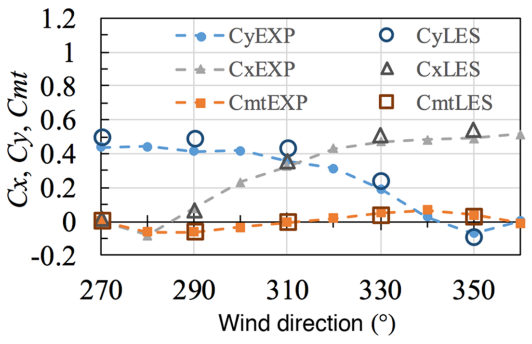


Figure 15. Comparison of average wind force coefficient (*Cx*, *Cy*) and torsional moment coefficient (*Cmt*)

3.2 Wind force evaluation for a base isolated office building

This is an example of LES for a base-isolated office building in an urban area (Yamanaka *et al*., 2014). The wind loads were evaluated using wind tunnel test results on a square cylinder performed in the past. When the building was in a city block, the influence of adjacent buildings was checked using LES to confirm that the wind force did not exceed the value of the building standing alone. An overview of the structure-grid-based LES solver is presented in Table 3 (Kataoka, Ono and Enoki, 2020).

Figure 16 shows the building to be analyzed and a model of the surrounding block. The target building was reproduced using a grid of two general curvilinear coordinate systems, and a high grid resolution in the vicinity of the building surface was achieved. In contrast, the peripheral building shapes were discretized using an orthogonal equidistant grid system. Accordingly, the boundary condition is satisfied by applying an external force to the equation of motion using the immersed boundary method (Goldstein *et al*., 1993).

Table 3. Outline for LES code "Aerodyna®" using structured grids

Item	Description
Solution algorithm	Fractional step method.
Control volume	Structured finite control volume (Over-lapping, general curvilinear coordinate system).
Discretization scheme (time)	3rd order Runge-Kutta for convective term. Crank-Nicolson for the viscous term.
Discretization scheme (space)	High-order interpolation for convective term. 2nd order central difference for viscous term.
SGS model	Dynamic-Mixed model.
Wall boundary condition	Two-layer model (Werner and Wengle).
Inflow	Semi-periodic + long fetch over roughness elements (RLBAIJ category III)

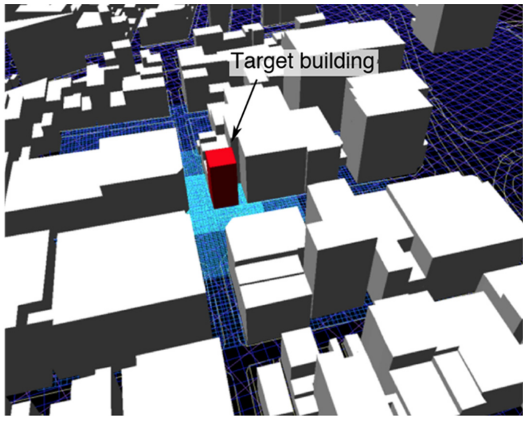


Figure 16. Computational model.

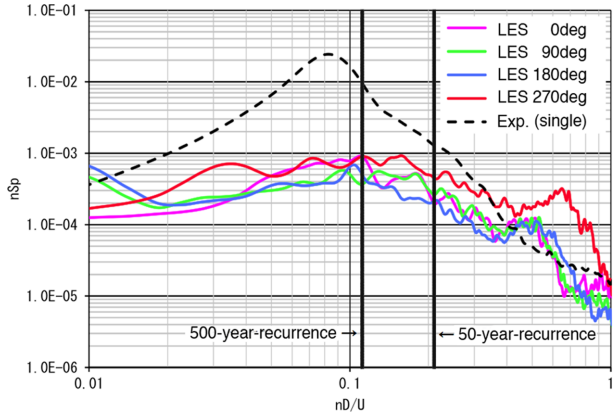


Figure 17. Power spectrum of fluctuating overturning moment coefficients.

Figure 17 presents the results of the power spectrum of the fluctuating overturning moment coefficients in four wind directions: 0°, 90°, 180°, and 270°, collectively with the results of the wind tunnel experiment on a building standing alone. The power of the fluctuating overturning moment coefficient associated with the wind force in the across-wind direction was reduced by the influence of the surrounding buildings. However, in the case of the wind direction 270°, it becomes stronger than the single building in the high-frequency range. In this wind direction, as depicted in Figure 18, the separated flow from the windward high-rise building accelerated along the street, impinged against the side of the target building, and caused an increase in the fluctuating overturning moment of the target building. This is also the influence of the surrounding buildings.

As a result of LES, it was confirmed that the surrounding buildings amplify the fluctuating wind force associated with the daily wind. Therefore, a tuned mass damper (TMD) was installed to reduce the vibration due to daily wind and improve habitability. The combination of wind tunnel experiments and CFD is highly effective at the early design stage.

4. Examination by CFD for other issues

Snow accretion on outer walls and high-temperature exhaust from emergency generators are introduced as examples of CFD application to other problems related to high-rise building planning.

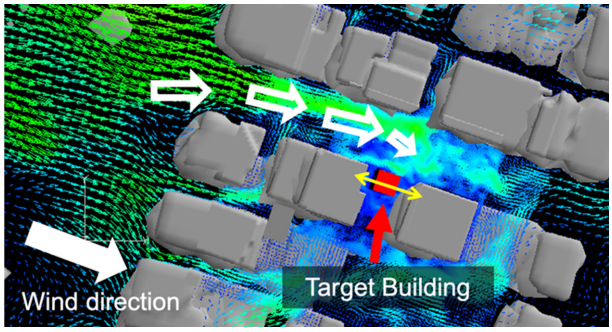


Figure 18. Flow visualization. (wind direction of 270°)

4.1 Snow accretion on exterior claddings

Fins and louvers are being increasingly installed on the exterior wall surfaces of high-rise buildings to prevent the heat loads caused by solar radiation from entering the interior. Besides causing unstable aerodynamic vibrations in strong winds, the exterior claddings can also be a source of wind-induced aeroacoustic noise. These phenomena have been investigated using wind tunnel testing, which provides results more easily than CFD. For example, wind-induced aeroacoustic noise generation can be verified by placing a component in a wind tunnel. The effectiveness of countermeasures, such as minor modifications to

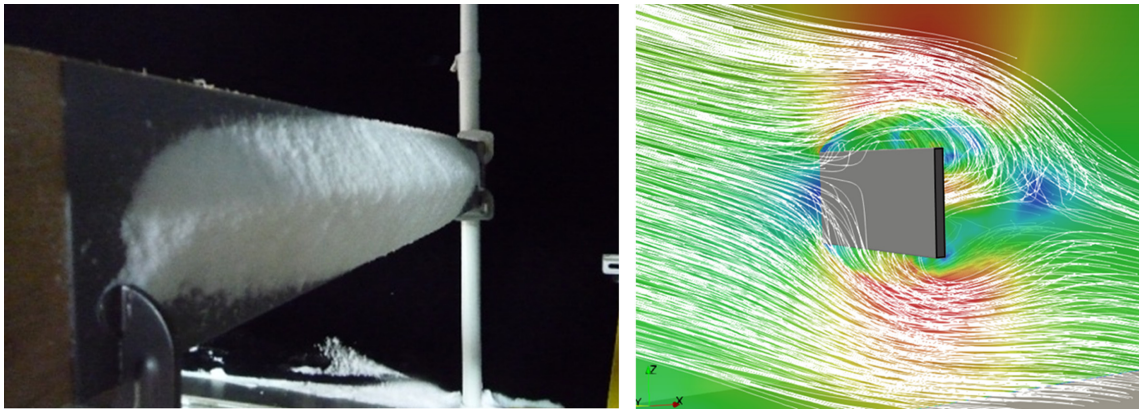


Figure 19. Snow accretion on a flat plate by experiment (left) and trajectory of snow particles by CFD (right).

geometry, can also be checked promptly.

Snow accretion on the exterior cladding has become a novel problem. The snow that adheres to the exterior claddings may fall in chunks due to its own weight or following a temperature rise, causing damage to the surrounding area. However, this issue has not yet been fully examined. As an exploratory study example, the prediction of snow accretion on exterior claddings is illustrated.

Figure 19 illustrates an example of snow accretion on a flat plate reproduced in a snowfall wind tunnel and the trajectory of snow particles around the flat plate obtained using CFD (Tabata and Otsuka, 2017). The trajectory of snow particles was obtained using the Lagrangian method for particles with a mass falling in the time-dependent flow field. Snow accretion on the flat plate had a triangular cross-sectional shape, with the position of its apex slightly higher than the center of the flat plate. Considering the trajectory of the snow particles, the stagnation point was located slightly higher than the center, which almost corresponds to the experiment.

Figure 20 presents a comparison of the distributions of the snow particle collision density on the building walls by changing the building width D. In this case, the time-averaged flow field obtained using RANS was used. In the case of D = 10 m or 80 m, a high-density range along the rim of the wall was clearly discernible, primarily because the airflow around the building carries snow particles to the periphery of the wall before they hit the front. This feature of the collision density distribution is quite similar to the general tendency of snow adhesion distribution on building walls facing wind, as observed in outdoor surveys (Tabata and Otsuka, 2017). In the case of the flat plate (D = 0.2 m, a narrower width allows snow particles to strike before they are blown away.

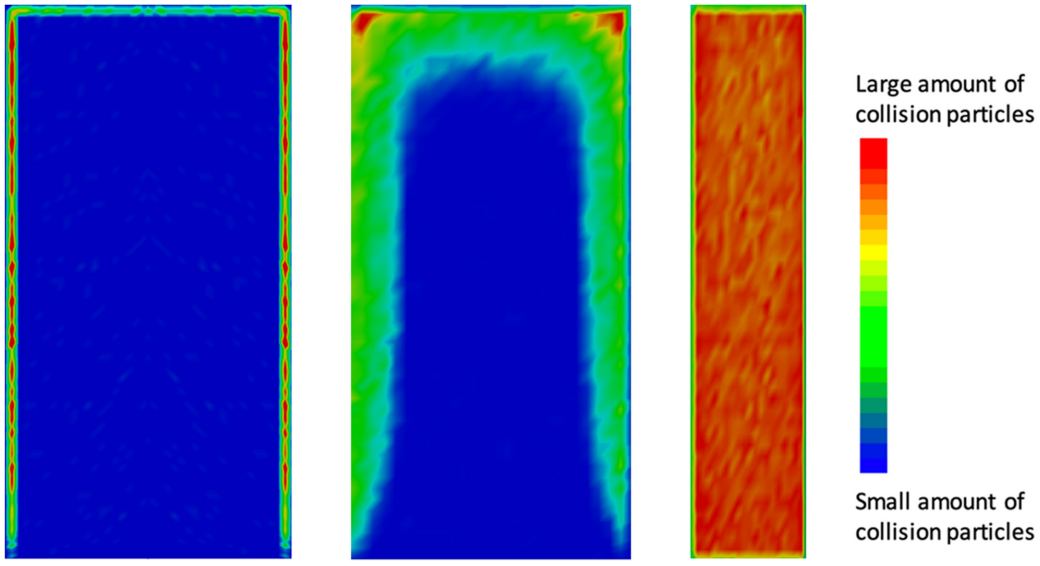
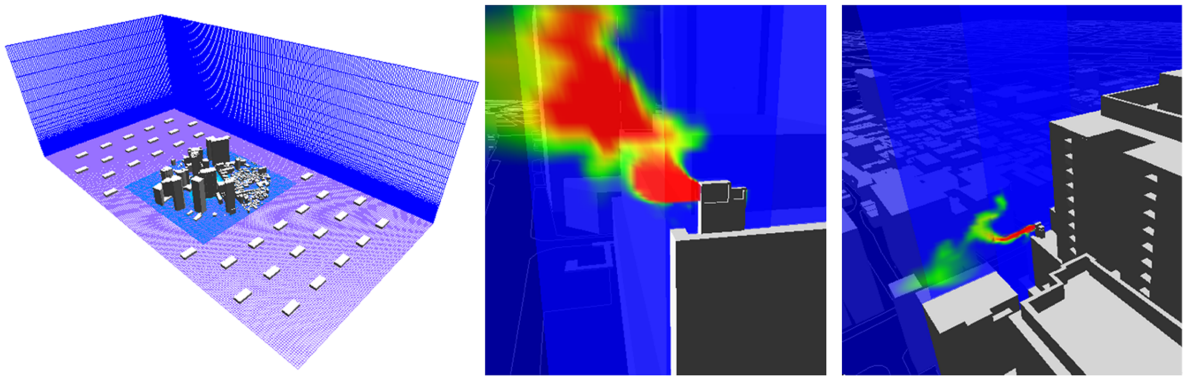


Figure 20. Distributions of snow particle collision density on building walls.



a) Computational domain b) Snapshots of the instantaneous temperature distributions

Figure 21. High temperature exhaust gas flows inside the urban canopy.

4.2 High temperature exhaust gas flow from Emergency Generator

An emergency generator (EG) system is indispensable to a company's business continuity plan (BCP). Their exhaust is usually located at the top of buildings, but some are not. Owing to the turbulence of the airflow within the urban canopy, the exhaust diffused irregularly. High-temperature exhaust gases can damage the exterior walls of buildings.

Figure 21 shows an LES example for predicting high-temperature exhaust gas flows from the middle floor of a building (Kataoka, Ono and Enoki, 2020). Exhaust from the emergency generator at 585°C was released from the chimney of the planned building surrounded by high-rise buildings. The entire domain size was 1.2 km wide x 2.4 km long × 0.8 km high (Fig. 21a). The reference wind velocity and wind direction were 10 m/s and NNW, respectively. From Figure 21b, intermittent and unsteady exhaust flows were observed. The time-averaged and maximum instantaneous air temperature distributions near the wall surfaces were evaluated based on the results.

5. Future prospects in using CFD

As described in Section 2.1, CFD and wind tunnels for predicting pedestrian wind environments are used according to the size of the target building and the planning stage. We believe that the same situation will occur in wind force evaluation. Specifically, structural wind forces are evaluated by CFD at early stages of structural design, and the final shape is examined by a wind tunnel along with the wind load evaluation for cladding. Alternatively, it may be possible to evaluate the wind force by CFD for small-to medium-sized buildings that are designed with only the values specified in the standards without experiments. Because only some simple shapes are described in the standards, verifying the actual shape using CFD contributes to wind safety.

There are still many phenomena for which CFD predictions are difficult to solve, even though they can be easily verified by wind tunnel experiments. Wind-induced aeroacoustic noise and its reduction is one such example, as mentioned in Section 4.1. However, a combination of CFD and wind tunnel experiments has become popular.

Problems to be solved exist in the present situation (Kataoka, Ono and Enoki, 2020). The most tedious task is to create a computational model of a building using building information modeling (BIM). It is necessary to eliminate unnecessary data for modeling and modify inconsistent shape definitions. The more complex the shape of a building, the greater the possibility of such inconsistencies. Therefore, creating a computational grid is another problem. An unstructured grid can be used to create a computational grid that is best suited for complex building geometries. However, in a concave space, such as a balcony or in a narrow gap, the boundary layer grid becomes distorted, and it becomes difficult to provide a sufficient number of grid points. Furthermore, when performing calculations for different wind directions, it is necessary to recreate the grid in each direction. These tasks are still difficult to perform automatically and are labor-intensive.

6. Conclusions

Application examples of CFD at the planning stage of high-rise buildings were introduced. The results were obtained for both environmental and structural design purposes. Moreover, snow accretion on exterior claddings and high-temperature exhaust gas flow from the emergency generator were illustrated. Finally, future prospects are described. Although some unresolved problems remain in using CFD, we expect that these problems will be resolved in the near future, and CFD will be applied to various areas for planning high-rise buildings.

Acknowledgments

The authors are grateful to Dr. K. Otsuka, Mr. S. Goto, and other department members at Obayashi Corporation

for their kind cooperation in daily research. The authors express their profound gratitude to Prof. Emer. Y. Tamura (Tokyo Polytechnic University), Prof. Emer. A. Wada (Tokyo Institute of Technology), and Mr. M. Nakai (Takenaka Corporation) for providing us with this honorable opportunity.

References

Kataoka, H., Ono, Y. and Enoki, K. (2020). Applications and prospects of CFD for wind engineering fields, Journal of Wind Engineering and Industrial Aerodynamics, 205, 104310.

Kataoka, H., Kinashi, S. and Kawaguchi, A. (2002). Development of "Zephyrus": A numerical simulator for wind environment, Report of Obayashi Corporation Technical Research Institute, 64, 49-54, https://www.obayashi.co.jp/technology/shoho/064/64-09.pdf, (in Japanese).

Hirt, C. W. (1992). Volume-fraction techniques: Powerful tools for wind engineering, Journal of Wind Engineering, 52, 333-344.

Kato., A., Mochida, A. Yoshino, H. and Murakami, S. (2001). "Numerical prediction of flow around tree by k-e model incorporating effects of plant canopy." Summaries of Technical Papers of Annual Meeting, Architectural Institute of Japan, D-1, 929-930, (in Japanese).

Yoshie, R., Mochida, A., Tominaga, Y., Kataoka, H., Hrimoto, K., Nozu, T. and Shirasawa, T. (2007). Cooperative project for CFD prediction of pedestrian wind environment in the Architectural Institute of Japan, Journal of Wind Engineering and Industrial Aerodynamics, 95, 1551-1578.

Tominaga, Y., Mochida, A., Yoshie, R., Kataoka, H., Nozu, T., Yoshikawa, M. and Shirasawa, T. (2008). AIJ guidelines for practical applications of CFD to pedestrian wind environment around buildings, Journal of Wind Engineering and Industrial Aerodynamics, 96, 1749-1761.

Murakami, S., Iwasa, Y. and Morikawa, Y. (1983). Investigation of statistical characteristics of wind at ground level and criteria for assessing wind-induced discomfort -part III Criteria for assessing wind-induced discomfort, Journal of Architectural Institute of Japan, 325, 74-84, (in Japanese).

Kinashi, S., Ono, Y., Kataoka, H. and Kawaguchi, A. (2005). Technical approaches for urban wind environment, Report of Obayashi Corporation Technical Research Institute, 69, https://www.obayashi.co.jp/technology/shoho/069/2005_069_11.pdf, (in Japanese).

Architectural Institute of Japan, (2015) AIJ Recommendations for Loads on Buildings, Maruzen, Tokyo, Japan, (in Japanese).

Kinashi, S., Tambara, C., Akagawa, H. and Kataoka, H. (2018). Wind environmental assessment for outdoor space around a building, Report of Obayashi Corporation Technical Research Institute, 82, https://www.obayashi.co.jp/technology/shoho/082/2018_082_46.pdf, (in Japanese).

Kataoka, H., Otsuka, K., Akagawa, H., Ono, Y. and Kawaguchi, A. (2009). Development of "Appias": a numerical urban climate simulator, Report of Obayashi Corporation Technical Research Institute, 73, https://www.obayashi.co.jp/technology/shoho/073/2009_073_09.pdf, (in Japanese).

Nakanishi, M. (2001). Improvement of the Mellor-Yamada turbulence closure model based on Large-Eddy simulation data, Boundary-Layer Meteorology, 99, 349-378.

Kataoka, H. and Tamura, T. (2012). Study on the relationship between roughness parameters and vertical wind velocity profiles over an urban area by LES, Journal of Structural and Construction Engineering (Transactions of AIJ), 77, 1203-1210, (in Japanese).

Enoki, K. and Ono, Y. (2016). "The prediction of wind loads acting on a building with complex surface using large eddy simulation and its validation." Summaries of Technical Papers of Annual Meeting, Architectural Institute of Japan, B-1, 229-230 (in Japanese).

Yamanaka, M., Kishi, H., Dochi, H., Sadahiro, M., Saito, M. and Ono, Y. (2014). Taisei Yaesu Building, MENSHIN 85, 3-8 (in Japanese).

Goldstein, D., Handler, R. and Sirovich, L. (1933). Modeling a no-slip flow boundary with an external force field, Journal of Computational Physics 105, 354-366.

Tabata, Y. and Otsuka, K. (2017). "Numerical simulation for predicting snow accretion distribution on building wall." Proceedings of 9th Asia-Pacific Conference on Wind Engineering.